Barrier Crossing in a Viscoelastic Bath

Félix Ginot,[1,*] Juliana Caspers,[2] Matthias Krüger,[2] and Clemens Bechinger[1]
[1]Fachbereich Physik, Universität Konstanz, 78457 Konstanz, Germany
[2]Institute for Theoretical Physics, Georg-August Universität Göttingen, 37073 Göttingen, Germany

(Received 31 August 2021; accepted 30 November 2021; published 11 January 2022)

We investigate the hopping dynamics of a colloidal particle across a potential barrier and within a viscoelastic, i.e., non-Markovian, bath and report two clearly separated timescales in the corresponding waiting time distributions. While the longer timescale exponentially depends on the barrier height, the shorter one is similar to the relaxation time of the fluid. This short timescale is a signature of the storage and release of elastic energy inside the bath that strongly increases the hopping rate. Our results are in excellent agreement with numerical simulations of a simple Maxwell model.

DOI: 10.1103/PhysRevLett.128.028001

The activated, i.e., fluctuation-assisted, hopping of a Brownian particle across an energy barrier ΔU is a paradigmatic and fundamental process with important applications across science, including chemical reactions [1–3], protein folding [4–8], nanomagnetic domain reversal [9], drug absorption [10], and voltage lifetimes, that has natural extensions to quantum tunneling phenomena [11]. The celebrated Kramers theory (see, e.g., Ref. [11] for a review) predicts the hopping rate $\nu \propto \exp(-\Delta U/k_B T)$ with $k_B T$ the thermal energy [1] in agreement with experimental observations. Many natural or technological systems, however, cannot be described in terms of a single degree of freedom. Under such conditions, the averaging out of degrees of freedom is nontrivial and typically leads to memory effects [12]. Several studies considered the crossing dynamics of a Brownian particle in a bath with memory [13–23]. When the bath is fully equilibrated prior to each barrier crossing, non-Markovian rate theory (NMRT) predicts a Kramers-like behavior, i.e., an exponential dependence of the hopping rate on the barrier height but with ν being considerably larger compared to an estimate based on the zero frequency memory kernel [14–16]. Such behavior is confirmed by simulations [23] and recent experiments [24]. However, considering that a hopping particle leads to permanent excitation of the bath, the assumption of an equilibrated bath is not necessarily valid.

In this work, we experimentally investigate barrier crossing of a Brownian particle in a double-well potential suspended in a viscoelastic solvent that exhibits non-Markovian behavior, i.e., pronounced memory. For potential barriers up to several $k_B T$, we find the hopping dynamics to be characterized not by one but *two* timescales that can differ by more than 2 orders of magnitude. While the long timescale increases exponentially with ΔU in agreement with the NMRT, the short one is almost unaffected by the barrier height. The latter results from elastic energy fluctuations of the viscoelastic bath due to excitations arising from the particle's hopping motion. Our results, which are in agreement with a simple model where the fluid is described as a Maxwell medium, have immediate consequences for the above examples, e.g., altering the interpretation and prediction of lifetimes.

We perform our experiments using silica particles with diameter 2.73 μm suspended in a 100 μm thick sample cell containing a viscoelastic fluid of a 5 mM equimolar aqueous solution of cetylpyridinium chloride monohydrate (CPyCl) and sodium salicylate (NaSal). The entire sample cell was kept at 25 °C where the fluid forms an entangled network of giant wormlike micelles [25] leading to viscoelastic behavior with a relaxation time ~0.7 s and zero-shear viscosity $\eta \approx 15$ mPa s determined by microrheology (methods are available in [26] and [27]). The particle is optically trapped by a 1064 nm laser beam with intensity 20 mW. Under such conditions, no heating effects are observed. More information regarding sample preparation, characterization, and stability is available in the Supplemental Material (SM) [28]. To yield double-well potentials with adjustable barrier, asymmetry, and well distance, the beam is periodically deflected by a galvanostatically driven mirror at a frequency of 400 Hz, and the intensity of the laser beam is modulated with a phase-locked acousto-optic modulator [Fig. 1(a)]. The shape of the potential U and in particular ΔU are measured from the particle's positional probability distribution in equilibrium [Fig. 1(c)]. Note that the two wells are connected by a thin potential energy corridor along the x direction so that we use a one dimensional analysis in the following. To avoid particle interactions with the surface, the optical potential was positioned in the midplane of the sample cell. Time-dependent particle positions were obtained with an uncertainty of ±6 nm from imaged video pictures taken with a frame rate of 200 Hz and using a custom Matlab [29] algorithm (see the SM). Each experimental run is 3–5 h long, and for every potential barrier height value, we

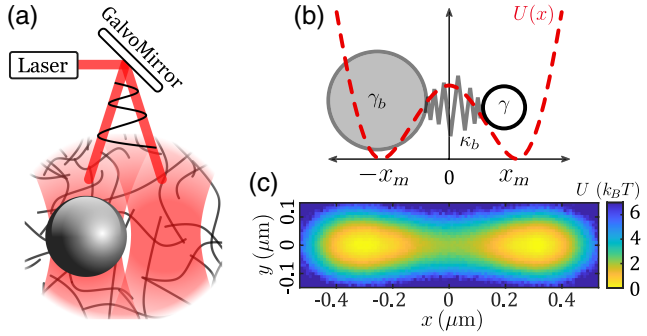

FIG. 1. (a) Experimental setup. A focused laser beam is deflected by a scanning mirror creating a double-well potential for a 2.73 μm silica tracer particle suspended in a viscoelastic solution of CPyCl-NaSal. (b) Sketch of the numerical model. A tracer particle with friction coefficient γ is subjected to a double-well potential $U(x)$. To account for the viscoelastic bath, it is coupled with linear spring of stiffness κ_b to a bath particle with friction coefficient γ_b. (c) 2D experimental potential measured from the probability density function $P(x, y)$ of the tracer.

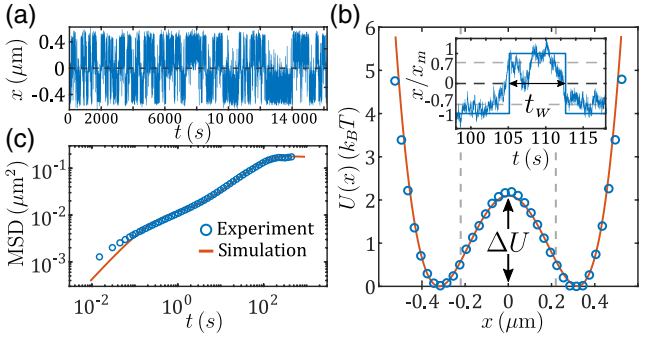

FIG. 2. (a) Trajectory $x(t)$ of a colloidal particle in a viscoelastic fluid and subjected to a double-well potential ($\Delta U = 2.1 k_B T$) for experiments. (b) Corresponding potential obtained from experimental data (blue circles) and a fit to Eq. (1), used in simulations (red line). Inset: The particle must pass the thresholds $\pm x_c = \pm 0.7 x_m$ to be considered as a crossing event with the waiting time t_w. (c) Mean square displacement of the colloidal particle obtained from experiments (blue circles) and simulations (red line). Model parameters (γ, γ_b, and κ_b) have been adjusted to optimize agreement with the experiments.

accumulate several experiments for a typical full duration of ~15 h.

Before discussing our experimental results, we introduce our theoretical model. A tracer (position x) with friction coefficient γ, which mimics the colloidal particle, is subjected to a double-well potential [30],

$$U(x) = -2\Delta U \left(\frac{x}{x_m}\right)^2 + \Delta U \left(\frac{x}{x_m}\right)^4, \tag{1}$$

with $\pm x_m$ being the positions of the potential minima and barrier height ΔU. (This form is in agreement with our experimental data [Fig. 2(b)]. The coupling of the tracer to the viscoelastic bath is modeled by a so-called bath particle (friction coefficient γ_b), which is connected to the tracer via a harmonic spring with stiffness κ_b [Fig. 1(b)]. This corresponds to the well-known Maxwell model. The Langevin equations for the positions x and x_b of tracer and bath particles thus read

$$\gamma \dot{x}(t) = -\kappa_b (x - x_b) - \nabla U + \xi(t) \quad \text{and} \tag{2}$$

$$\gamma_b \dot{x}_b(t) = -\kappa_b (x_b - x) + \xi_b, \tag{3}$$

where ξ and ξ_b are delta correlated random forces with zero mean $[(\xi_i, \xi_j) \in \{\xi, \xi_b\}]$,

$$\langle \xi_i(t) \rangle = 0, \qquad \langle \xi_i(t) \xi_j(t') \rangle = \delta_{ij} 2 k_B T \gamma_i \delta(t - t'). \tag{4}$$

Note that these coupled equations can be combined into one non-Markovian Langevin equation for x with memory kernel $\Gamma(t) = 2\gamma\delta(t) + \kappa_b \exp[-(\kappa_b/\gamma_b)t]$. Since we are also interested in the explicit position of the bath particle, we will explicitly solve the set of Eqs. (2) and (3).

Figure 2(a) shows an experimentally measured tracer trajectory $x(t)$ in a double-well potential with $\Delta U = 2.1 k_B T$ and minima positions $\pm x_m = \pm 0.32$ μm. During the plotted time interval of ~4.5 h, approximately 200 barrier crossings are observed. From the trajectories and the corresponding positional probability distribution, we compute the external potential $U(x)$ [Fig. 2(b)] and the mean square displacement (MSD) [Fig. 2(c)]. Comparing the experimental data with the results of Eqs. (2) and (3), we obtain the parameters $\gamma = 0.189$ μNs/m, $\gamma_b = 1.44$ μNs/m, and $\kappa_b = 0.4$ μN/m, which yields the relaxation times of the tracer and bath particles $\tau = (\gamma/\kappa_b) = 0.5$ s and $\tau_b = (\gamma_b/\kappa_b) = 3.6$ s, respectively. We have experimentally confirmed that these parameters do not depend on ΔU (see the SM).

To analyze the hopping dynamics of the tracer particle, we calculated the probability distribution $P(t_w)$ of waiting times t_w, i.e., the time between two consecutive barrier crossing events. A barrier crossing event is defined by the colloid successively passing two thresholds at positions $\pm x_c = \pm 0.7 x_m$. In Fig. 2(b) (inset), we show two crossing events (at $t \sim 105$ s and $t \sim 112$ s) and the time t_w the particle stays in the right well. Because the choice of x_c affects $P(t_w)$, identical thresholds have been applied when analyzing experimental and numerical data.

Figure 3(a) shows $P(t_w)$ for $\Delta U = 2.1 k_B T$. Apart from a sharp increase at short timescales that is caused by the finite well distance, a monotonic decrease in $P(t_w)$ is observed. Experiments (blue symbols) and simulations (red solid line) are well described by a superposition of two exponential decays, with timescales τ_s (dashed black line) and τ_l (full black line):

$$P(t_w) = \frac{A_s}{\tau_s} \exp\left(-\frac{t_w}{\tau_s}\right) + \frac{A_l}{\tau_l} \exp\left(-\frac{t_w}{\tau_l}\right). \tag{5}$$

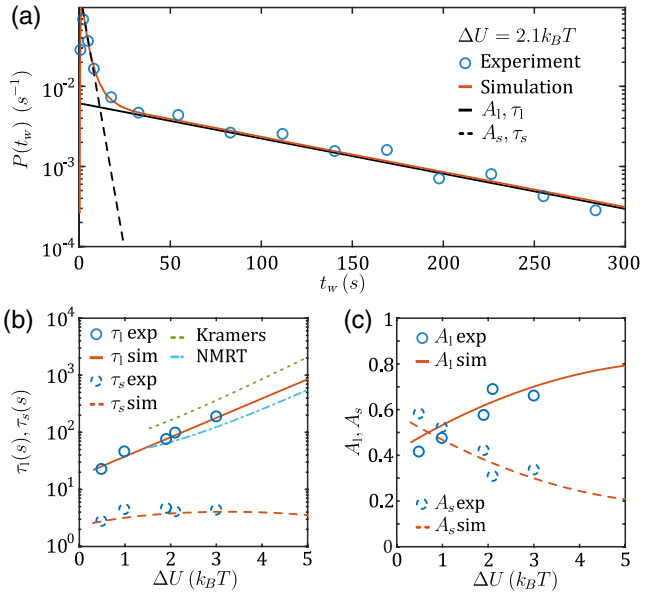

FIG. 3. (a) Waiting time distribution $P(t_w)$ in a double-well potential ($\Delta U = 2.1 k_B T$) for experiments (blue circles) and simulations (red line). Both show a double-exponential decay with timescales τ_s and τ_1 and amplitudes A_s and A_1, respectively. Dashed and full black lines highlight the short and long timescales. (b) Short τ_s (dashed lines) and long timescales τ_1 (full lines) for experiments (blue circles) and simulations (red lines) in double-well potentials with varying ΔU. Green dotted and light blue dash-dotted lines correspond to theoretical predictions according to Kramers and the NMRT. (c) Amplitudes $A_{s/l}$ of short (dashed lines) and long (full lines) timescales τ_s and τ_1 for different ΔU. Blue circles correspond to experiments, red lines to simulations.

To yield a normalized probability distribution, we set $A_s + A_1 = \int_0^\infty dt P(t) \equiv 1$. Accordingly the amplitudes in Eq. (5) denote the fraction of short and long waiting times in the hopping dynamics. The corresponding decay times and amplitudes obtained from fitting Eq. (5) to experimental and numerical data are shown in Figs. 3(b) and 3(c). Opposed to τ_s, which only slightly varies with ΔU, an exponential dependence on ΔU (qualitatively similar to the Kramers prediction, green dotted line) is observed for τ_1. Note the good agreement with the NMRT, which is plotted as dash-dotted line in Fig. 3(b). By definition, the amplitudes of the fast and slow decay exhibit an opposite dependence, with A_1 monotonically increasing with ΔU.

For a qualitative understanding of the two timescales, we note that the friction coefficient of the bath particle is much larger than that of the tracer. Therefore, the bath particle cannot immediately follow a tracer's jump across the barrier. This leads to an additional elastic force on the tracer *immediately* after a barrier crossing event (e.g., from left to right), which lowers the effective potential barrier. As a result, the probability for an *immediate* jump back (to the left well) increases, which explains the short waiting times in our experiments. If the tracer misses such an opportunity but remains longer in the (right) well than τ_b, the fluid relaxes. Then, the elastic force vanishes, which again increases the effective potential barrier and thus leads to long waiting times. A hopping event under such conditions is comparable to that in an equilibrated system, which explains why τ_1 exhibits a Kramers-like dependence on ΔU. As a consequence, the fraction of fast hopping events A_s will increase with decreasing ΔU where the tracer's hopping dynamics becomes increasingly faster than τ_b in agreement with Fig. 3(c). When hopping events are rare ($\Delta U \gg k_B T$), the bath particle is likely to equilibrate prior to another tracer's barrier crossing event. Accordingly, the amplitude of the short timescale decays to zero [Fig. 3(c)].

To provide direct evidence for a time-dependent effective potential acting on the colloidal particle, in a first step we have calculated the time-independent total force F acting on it. It is obtained from its short-time drift motion [12]:

$$F(x) = \gamma_\infty \lim_{\delta t \to 0} \int dl \frac{l}{\delta t} P(x + l, \delta t | x, 0), \tag{6}$$

where γ_∞ is the colloid's short-time friction coefficient. $P(x, t|x', t')$ is the conditional probability to find the particle at position x at time t given it was at position x' at t'. The corresponding effective potential is then given by $U(x) = -\int^x F(x')dx'$. Experimentally, the value of γ_∞ is obtained by comparing $U(x)$ using integration of Eq. (6) with the equilibrium potential shown in Fig. 2(b). For the simulations naturally $\gamma_\infty = \gamma$. To consider memory effects in the effective force acting on the particle, we replace the two-point probability in Eq. (6) by the three-point conditional probability $P(x + l, \delta t | x, 0; x_{-t}, -t)$, which adds the additional constraint that the particle was located at position x_{-t} at a time interval t *prior* to $t = 0$, where the particle was at position x. As a result, the drift force depends also on the time interval t. The difference between $F(x, -t) \equiv F(x, t)$ and $F(x)$ is then a direct measure of the non-Markovianity of the viscoelastic bath.

Figure 4 shows the corresponding total time-dependent pseudopotential acting on the tracer $U_{\text{eff}}(x, t) = -\int^x F(x', t)dx'$ under the initial condition that it was located at time interval t *prior* to $t = 0$ in the left potential well, i.e., $x_{-t} \leq -x_c$. In agreement with our above qualitative explanation, the potentials are strongly asymmetric at short times due to the presence of elastic forces acting on the tracer. With increasing t, elastic forces gradually decrease until the symmetric optical double-well potential is recovered. As an immediate consequence, the mean distance $\langle x_b(t) \rangle - x$ should decrease with increasing t. As an example, we show as vertical arrows in Fig. 4 how $\langle x_b(t) \rangle$ gradually approaches $x = 0.7 x_m$ with increasing t. The elastic energy corresponding to the mean tracer-bath particle distance, $U_{\text{el}} = 1/2 \kappa_b (\langle x_b(t) \rangle - 0.7 x_m)^2$ after $t = 1$ s yields $2.1 k_B T$ (orange arrow in Fig. 4), which also

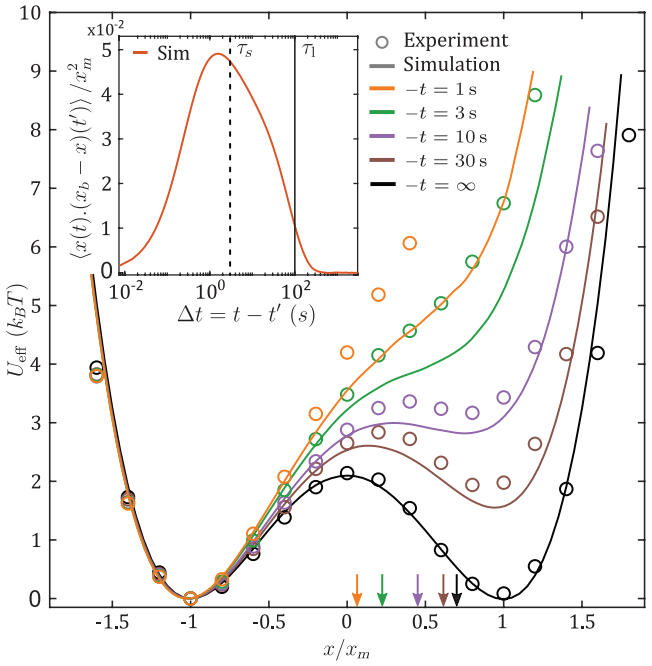

FIG. 4. Effective pseudo potentials $U_{\mathrm{eff}}(x,t)$ for experiments (circles) and simulations (lines) in a double-well potential ($\Delta U = 2.1 k_B T$). For $t \to \infty$, $U_{\mathrm{eff}}(x,t)$ (colors) relaxes to U (black). The arrows highlight the average bath particle position $\langle x_b \rangle$ given the tracer sits at $x = 0.7 x_m$ with (colors) or without (black) conditioning on being in the left well t seconds earlier. Inset: Cross-correlation $\langle x(t)(x_b - x)(t') \rangle$ between tracer position x and bath-tracer distance $x_b - x$. The cross-correlation is largest for $\Delta t = t - t' \sim \tau_s$ and decays to zero for $\Delta t \gg \tau_1$.

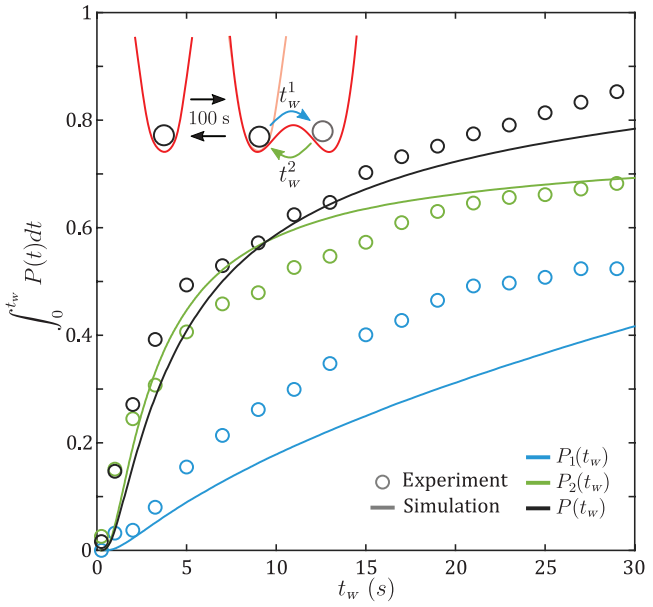

FIG. 5. Integrated waiting time distributions $P_1(t)$ and $P_2(t)$ for experiments (circles) and simulations (lines) according to the protocol shown in the inset and explained in the text. Black curve and symbols correspond to the previous situation of a static double-well potential [such as in Fig. 2(b)]. Light blue and green data correspond to first and second particle jumps after release of the particle from a single potential well.

explains the disappearance of the barrier in the effective potential.

Interestingly, even for $t = 30$ s being considerably larger than the particle's relaxation times, a pronounced asymmetry in the effective potential is observed. This is understood by considering the cross-correlation $\langle x(t)(x_b - x)(t') \rangle$ between tracer position x and bath-tracer distance $x_b - x$, which characterizes elastic correlations in the system (inset of Fig. 4). It decays after more than $t = 100$ s, corresponding to the longest timescale in our system τ_1 and thus explains the slow decay of the asymmetry in the effective pseudopotentials.

As an immediate consequence of Fig. 4, we demonstrate that when a hopping process starts from a fully equilibrated bath where no elastic energy is stored in the system, the short timescale disappears. For an experimental realization of such conditions, we have strongly suppressed the tracer's motion over 100 s, which largely exceeds the system's relaxation time. This was achieved by removing one potential well leading to a single harmonic particle trap (see inset in Fig. 5). Experimentally, we slightly (∼1%) decreased the right well laser intensity, creating a strong asymmetry in the system and confining the particle to the left well. Having established an equilibrium condition at $t = 0$, we suddenly restored the symmetric double-well potential and measured the waiting times of the first barrier crossing. Figure 5 shows the integrated waiting time distributions $\int_0^{t_w} P_1(t)dt$ of first particle crossings, which corresponds to the fraction of jumps occurring for $0 < t \leq t_w$. The data have been obtained from about 200 repetitions of the above protocol. Compared to the integrated waiting time distributions obtained in presence of a permanent double-well potential (black data), short waiting times are strongly suppressed under the constraint of an equilibrium initial state, which confirms that the asymmetry of U_{eff} results from the elastic energy stored in the bath. Interestingly, when considering the waiting times of the second crossing (P_2), corresponding to jumps back to the initial well, fast hopping events are almost completely restored (green data in Fig. 5). This demonstrates that after a single hopping event over the potential barrier, the elastic energy stored in the bath has already reached its maximal value. The simulations (solid lines) reproduce this behavior, even though quantitative differences are observed (see the SM).

In summary, with experiments and simulations we have investigated the hopping dynamics of an overdamped colloidal particle over an energy barrier in the presence of a viscoelastic bath. Compared to a purely viscous, i.e., memory-free, solvent, where the hopping dynamics is governed by the Kramers rate, we find two timescales in the waiting time distribution for a non-Markovian bath leading to a rather fast surmounting of energy barriers as

large as $3k_BT$. The larger timescale τ_1 displays an exponential dependence on the potential barrier height ΔU in agreement with the NMRT. On the opposite, the shorter timescale τ_s is caused by the permanent excitation of the bath due to the hopping motion of the tracer and is rather independent of the barrier height. Because this fast process is governed by the slow equilibration of the bath particle, τ_s should be rather independent of the specific choice of the potential shape and therefore relevant under many conditions. In particular, in biological environments that are typically viscoelastic, we expect our results to be important for the correct interpretation of barrier heights derived from the particle's hopping dynamics.

We thank Matthias Fuchs for fruitful discussions and Jakob Steindl and Luis Reinalter for preparing micellar solutions and for performing rheological measurements. This project was funded by the Deutsche Forschungsgemeinschaft (DFG), Grant No. SFB 1432—Project ID 425217212. F. G. acknowledges support by the Alexander von Humboldt foundation.

*Corresponding author.
felix.ginot@uni-konstanz.de

[1] H. A. Kramers, Physica (Amsterdam) **7**, 284 (1940).
[2] P. L. García-Müller, F. Borondo, R. Hernandez, and R. M. Benito, Phys. Rev. Lett. **101**, 178302 (2008).
[3] G. R. Fleming, S. H. Courtney, and M. W. Balk, J. Stat. Phys. **42**, 83 (1986).
[4] M. Laleman, E. Carlon, and H. Orland, J. Chem. Phys. **147**, 214103 (2017).
[5] K. Neupane, A. P. Manuel, and M. T. Woodside, Nat. Phys. **12**, 700 (2016).
[6] W. Zheng and R. B. Best, J. Phys. Chem. B **119**, 15247 (2015).
[7] N. Socci, J. N. Onuchic, and P. G. Wolynes, J. Chem. Phys. **104**, 5860 (1996).
[8] R. Satija and D. E. Makarov, J. Phys. Chem. B **123**, 802 (2019).
[9] R. H. Koch, G. Grinstein, G. A. Keefe, Y. Lu, P. L. Trouilloud, W. J. Gallagher, and S. S. P. Parkin, Phys. Rev. Lett. **84**, 5419 (2000).
[10] M. Bernetti, M. Masetti, W. Rocchia, and A. Cavalli, Annu. Rev. Phys. Chem. **70**, 143 (2019).
[11] P. Hänggi, P. Talkner, and M. Borkovec, Rev. Mod. Phys. **62**, 251 (1990).
[12] H. Risken, in *The Fokker-Planck Equation* (Springer, New York, 1996).
[13] L. Rondin, J. Gieseler, F. Ricci, R. Quidant, C. Dellago, and L. Novotny, Nat. Nanotechnol. **12**, 1130 (2017).
[14] R. F. Grote and J. T. Hynes, J. Chem. Phys. **73**, 2715 (1980).
[15] P. Hanggi and F. Mojtabai, Phys. Rev. A **26**, 1168 (1982).
[16] B. Carmeli and A. Nitzan, Phys. Rev. A **29**, 1481 (1984).
[17] L. Lavacchi, J. Kappler, and R. R. Netz, Europhys. Lett. **131**, 40004 (2020).
[18] J. Kappler, V. B. Hinrichsen, and R. R. Netz, Eur. Phys. J. E **42**, 119 (2019).
[19] E. Medina, R. Satija, and D. E. Makarov, J. Phys. Chem. B **122**, 11400 (2018).
[20] J. Kappler, J. O. Daldrop, F. N. Brünig, M. D. Boehle, and R. R. Netz, J. Chem. Phys. **148**, 014903 (2018).
[21] R. Ianconescu and E. Pollak, J. Chem. Phys. **143**, 104104 (2015).
[22] E. Pollak, H. Grabert, and P. Hänggi, J. Chem. Phys. **91**, 4073 (1989).
[23] I. Goychuk, Phys. Rev. E **80**, 046125 (2009).
[24] B. R. Ferrer, J. R. Gomez-Solano, and A. V. Arzola, Phys. Rev. Lett. **126**, 108001 (2021).
[25] M. Cates and S. Candau, J. Phys. Condens. Matter **2**, 6869 (1990).
[26] J. R. Gomez-Solano and C. Bechinger, New J. Phys. **17**, 103032 (2015).
[27] R. Jain, F. Ginot, J. Berner, C. Bechinger, and M. Krüger, J. Chem. Phys. **154**, 184904 (2021).
[28] See Supplemental Material at http://link.aps.org/supplemental/10.1103/PhysRevLett.128.028001 for in-depth description of the experimental methods and analysis.
[29] J. C. Crocker and D. G. Grier, J. Colloid Interface Sci. **179**, 298 (1996).
[30] C. Schmitt, B. Dybiec, P. Hänggi, and C. Bechinger, Europhys. Lett. **74**, 937 (2006).